Applied Radiation and Isotopes 229 (2026) 112356

Contents lists available at ScienceDirect

Applied Radiation and Isotopes

journal homepage: www.elsevier.com/locate/apradiso

Gamma ray interaction studies on light-weight, eco-friendly PVA-based composites using construction waste materials as fillers

Ashwitha Chikkegowda [a], Adarsh Raj Lingaraj [a], Vaishnavi Narayan [a], Sankarshan Belur Mohan [b,*], Sannathammegowda Krishnaveni [a,**]

[a] Department of Studies in Physics, University of Mysore, Mysuru, 570006, India
[b] Department of Physics, The National Institute of Engineering, Mysuru, 570008, India

ARTICLE INFO

Keywords:
Gamma ray shielding
PVA-Composites
HVL
TVL
μ
μ/ρ
Z_{eff}

ABSTRACT

The search for alternatives to toxic lead-based shielding materials is vital for sustainable radiation protection. This study investigates polyvinyl alcohol (PVA) composites reinforced with recycled eco-friendly fillers: granite, glass, and redmud as substitutes for conventional gamma-ray shields. Shielding parameters, including Linear and Mass attenuation coefficients (μ, μ/ρ), Half value layer (HVL), Tenth value layer (TVL), Mean free path (λ), and Effective atomic number (Z_{eff}), were measured for composites with 10–40 wt% filler concentrations using gamma energies from 511 to 1332 keV. Experimental results closely matched theoretical values determined from XCOM and AutoZeff softwares. The findings show that increasing filler concentrations lead to an increase in μ, μ/ρ, and Z_{eff}, whereas decrease in HVL, TVL, and λ for all three PVA composites. The maximum value of μ/ρ i.e., 0.090, 0.089, and 0.082 cm^2/g is observed at 511 keV, and Z_{eff} i.e., 10.068, 8.527 and 7.988 at 1332 keV for 40 wt% filler concentration for PVA - Granite, PVA-Glass and PVA-Redmud, respectively. Furthermore, among the composites, PVA–granite exhibited the highest μ (0.28 cm^{-1}), μ/ρ (0.09 cm^2/g), and Z_{eff} (10.07), along with the lowest HVL (2.50 cm), TVL (8.31 cm), and λ (3.61 cm) values at 40 wt% for a given energy. These results highlight that PVA–granite acts as a relatively better shielding composite and serves as a promising, lightweight, flexible, and eco-friendly alternative for radiation shielding in medical, nuclear, and aerospace applications.

1. Introduction

Gamma radiation is a high-energy electromagnetic radiation emitted from atomic nuclei. The rapid advancement of science and technology has led to a widespread applications, due to its unique properties, particularly its strong penetrating ability, across diverse fields such as nuclear medicine, medical diagnostics, industrial processing, scientific research, and security (Hussain et al., 2022). Prolonged exposure to this ionizing radiation can be harmful for materials used in devices as well as for the living biome (Ahmad et al., 2021), and can increase the risk of developing genetic mutations, causing damage to blood cells and tissues and organ failure (Elgazzar and Kazem, 2014). Thus, an in-depth understanding of gamma-ray interactions with matter is essential for advancing radiation protection and dosimetry. Developing effective shielding materials has become a research priority in nuclear science and technology (Chmielewski, 2010; Alrowaili et al., 2025; Henaish et al., 2020). Traditionally, materials such as lead and lead-based composites, bismuth oxide, and tungsten have been used as gamma-ray shielding due to their high atomic numbers and densities, which make them effective at absorbing high-energy photons. However, these materials have considerable drawbacks as they are dense and heavy, which limits their applicability in scenarios where weight is a constraint. Additionally, lead being toxic, imposes environmental and health hazards during their handling, usage and disposal (Gual et al., 2018). Considering these limitations, alternative materials that are lightweight, non-toxic, cost-effective and flexible are increasingly desirable in radiation shielding applications.

Recent studies have shown a growing interest in developing sustainable and efficient materials for gamma radiation shielding. Structurally engineered composites used in construction have demonstrated promising photon attenuation capabilities. Novel absorbers synthesized from waste marble/polyester incorporating $PbCO_3$ and CdO have exhibited improved attenuation along with environmental benefits (Sayyed et al., 2022a), while the green conversion of hazardous CRT

* Corresponding author.
** Corresponding author. Department of Studies in Physics, University of Mysore, Manasagangothri, Mysuru, 570006, India.
E-mail addresses: bmsankarshan@gmail.com (S. Belur Mohan), sk@physics.uni-mysore.ac.in (S. Krishnaveni).

https://doi.org/10.1016/j.apradiso.2025.112356
Received 2 September 2025; Received in revised form 1 November 2025; Accepted 1 December 2025
Available online 1 December 2025

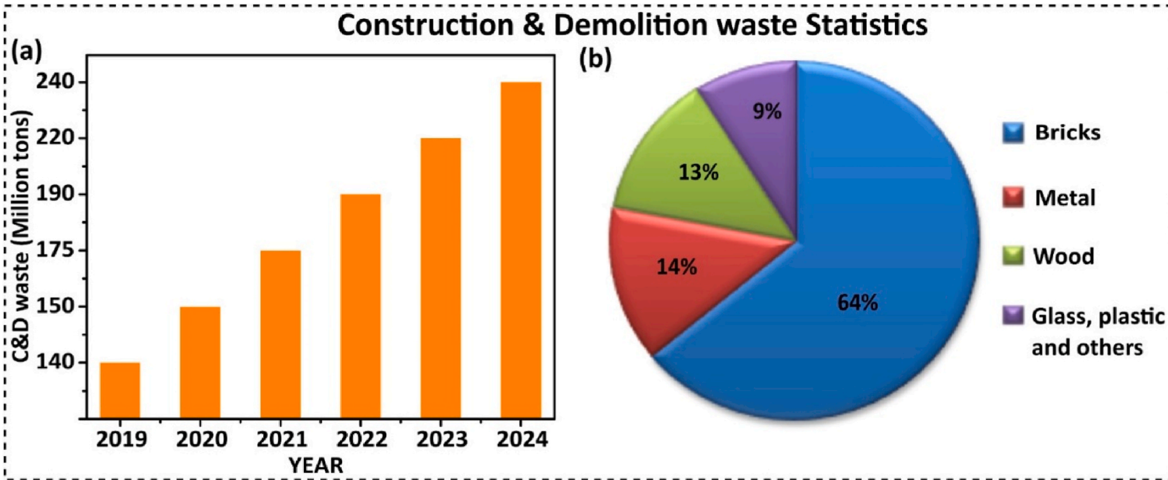

Fig. 1. (a) Annual trend of construction and demolition (C&D) waste generation and (b) corresponding material composition distribution.

waste and red mud into radiation-shielding concrete has underscored the potential of upcycling industrial waste (Sayyed et al., 2022b). Enhanced gamma attenuation has also been achieved in gypsum–lime–waste-marble mortars through micro/nano-PbO addition (Alabsy et al., 2023), and natural materials such as clays (Elsafi et al., 2021), local granites (Abdalla et al., 2022), heavy-mineral-doped clay bricks (Mahmoud et al., 2021), OPC pastes blended with glass wastes (Shwita et al., 2021), mineralized siltstone/dolostone formations (Aita et al., 2022), and even different wood species (Barman et al., 2022) have been evaluated for their radiation-shielding performance. Likewise, the gamma shielding properties of dental ceramics (Şengül et al., 2023) indicate that diversified natural and engineered materials can be effectively tailored for nuclear protection. In addition to construction materials, glass-based matrices, geopolymer binders, and advanced glass-ceramic compositions are being extensively investigated as promising Pb-free alternatives for gamma shielding. Bi_2O_3-doped recycled CRT glass exhibited improved density, microstructural refinement, and radiation energy absorption (Alzahrani et al., 2023), while metakaolin-based geopolymers containing borosilicate waste glass demonstrated favorable physicochemical and shielding properties (Alrowaili et al., 2024). Lead-oxide loading has been validated to enhance attenuation in newly developed geopolymer networks (Echeweozo et al., 2024), and apatite–wollastonite matrices modified with SiO_2, Fe_2O_3, and TiO_2 have shown competitive absorption behaviour (Elqahtani et al., 2025). Multi-component glass systems, including Pb–W–B glasses with Sb/Al/Bi modifiers (Katubi et al., 2024), silicon-rich Na_2O–SiO_2–Al_2O_3–CaO–ZnO glasses (Alzahrani et al., 2024), P_2O_5-based glasses (Katubi et al., 2023), and Ga-silicate systems (Alsaiari et al., 2025a), have demonstrated high shielding efficiency, with reviews confirming that modifier class critically governs attenuation and microstructural densification (Al-Buriahi et al., 2025). Furthermore, Bi_2O_3–Y_2O_3 co-doped glass-ceramics have exhibited enhanced nuclear shielding through improved structural compactness and high-Z loading (Alsaiari et al., 2025b). However, most glass, geopolymer, ceramic, and construction-derived shielding systems, though effective in attenuation, suffer from limitations such as high density, brittleness, rigidity, processing difficulty, and lack of flexibility or portability. Consequently, polymer-based composites are now emerging as attractive alternatives due to their low cost, light weight, ease of moulding or 3D forming, and versatile chemical stability, making them suitable candidates for next-generation flexible radiation-shielding applications (Singh and Kumar, 2019).

A range of polymers, including polyoxymethylene (POM), Natural rubber (NR), Poly methyl acrylate (PEA), Poly-phenyl-methacrylate (PPM) (Bhosale et al., 2017), Polyamide nylon-6 (PA-6), Poly-acrylonitrile (PAN), Poly-vinylidene chloride (PVDC), Poly-aniline (PANI), Polyethylene terephthalate (PET), Poly-phenylene Sulfide (PPS), Poly-pyrrole (PPy), Poly-tetrafluoro-ethylene (PTFE) (Kaçal et al., 2019), Poly-vinylidene chloride (PVC) (Yang et al., 2023) etc., have been investigated for their attenuation properties, revealing their potential in shielding applications. Among these polymers, polyvinyl alcohol (PVA) stands out due to its distinctive properties. PVA is a water-soluble synthetic polymer with favorable compressive and elastic mechanical properties (Issa et al., 2021). It is non-toxic, environmental-friendly, and has significant durability in ambient environments, making it a suitable candidate for radiation shielding, particularly in applications where weight and flexibility are critical (Thangprasert et al., 2019). Moreover, PVA's ability to dissolve in water facilitates eco-friendly disposal and recycling, further enhancing its appeal in green engineering (Chiang et al., 2024). Polymer composites have shown enhanced shielding efficacy when polymers are blended with suitable fillers. Various studies have demonstrated the benefits of incorporating fillers into the polymer matrix, such as PVA-Bentonite clay (Wang et al., 2013), PVC-bismuth vanadate (Singh et al., 2017), PVA-Red mud (metal oxide-rich waste) (Daw et al., 2019), PVA-dysprosium (III) oxide and erbium (III) oxide (Mostafa et al., 2022), PVA-yttrium oxide (Yu et al., 2007), PVA - Cadmium chloride (Baraker and Lobo, 2018), Polymethyl methacrylate (PMMA)-bismuth trioxide (Jia et al., 1999), PVC–polyethylene glycol (PEG)-polyvinyl Pyrrolidone (PVP) - zirconium oxide (Agool et al., 2017), PMMA-Colemanite (Bel et al., 2019), and Metalized polypropylene (MAPP)-newspaper fiber (Ashori and Sheshmani, 2010), etc., with increased attenuation capability compared to pristine polymer.

The choice of filler material is critical as it impacts the composite's density, atomic composition, and overall effectiveness in gamma-ray shielding. Additionally, incorporating fillers provides flexibility in designing lightweight and customizable materials for specific applications, making polymer composites an attractive area of study in radiation shielding. Therefore, from a sustainability perspective, the use of materials that are readily available, cost-effective and environmental friendly is highly desirable. In this regard, construction and demolition (C&D) waste represents an attractive filler resource, since vast quantities remain unutilized; valorizing such waste not only supports recycling and waste-management strategies, but also contributes to the development of greener, eco-friendly radiation shielding materials. Fig. 1 illustrates the annual generation and composition of C & D waste over the past six years, revealing an increase from about 140 million tons in 2019 to over 240 million tons in 2024. The most recent data indicates that these waste primarily comprises of bricks (64 %), metals (14 %), wood (13 %), and a mixture of glass, plastics, and other materials (9 %) (Sakthibala et al.,

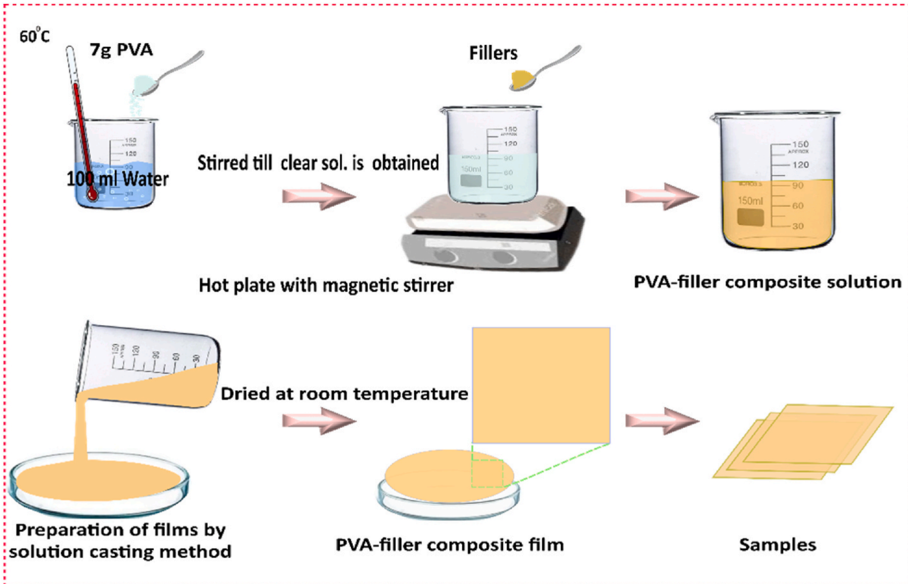

Fig. 2. Schematic representation of preparation of PVA composite films.

2025), (Bonifazi et al., 2025). Granite, which is an igneous rock, is a typical shielding material used in building construction because of their large attenuation cross-section for gamma rays (Pavlidou et al., 2006). Glass, primarily consisting of silica (SiO_2), which is commonly found in sand, is an emerging radiation shielding material (Issa et al., 2020; Madbouly et al., 2022; Alomayrah and Al-Buriahi, 2024). Redmud contains various oxides, such as oxides of iron, aluminum, silicon and titanium, which contribute to its moderate density and enable it as a sustainable candidate for radiation shielding (El-Khayatt and Saudi, 2024) (Salati et al., 2022). These materials are easily accessible from construction and demolition sites and are economical. In this context, the present work aims to address both the escalating issue of C&D waste generation and the need for economical, eco-friendly radiation shielding materials. To promote effective recycling of solid waste and simultaneously enhance the gamma-ray attenuation performance of polymer composites, filler powders such as granite, glass, and red mud, extracted from construction and industrial waste streams, were incorporated into the PVA polymer matrix. The selection of these materials is justified by their abundance, low cost, and high elemental density, making them suitable candidates for sustainable and efficient gamma-ray shielding applications.

2. Theory

Absorption and scattering phenomena are the main factors influencing the attenuation of gamma ray photons as they pass through an absorber (Chikkegowda et al., 2024a). When gamma radiation is incident on an absorber of thickness (t), intensity of the radiation decreases along the thickness of a material (Junior et al., 2017), (Krishnappa et al., 2023). The amount of incident radiation (I) attenuated when it passes through a material of thickness 't' is indicated by the linear attenuation coefficient (μ), given by,

$$I(x)\ \alpha\ e^{-\mu t} \tag{1}$$

Higher μ value indicates that the material is more effective at reducing radiation intensity and it depends on the sample composition (Watanabe, 1999). The reciprocal of μ is called the mean free path (λ), which is the average distance a gamma ray travels between collisions with atoms of target material (Basu et al., 2019). In essence, λ gives a natural concept of how far radiation can travel before being affected and μ quantifies the rate of attenuation.

$$\lambda = 1/\mu \tag{2}$$

The thickness at which the incident radiation reduces to half of its initial value is known as half value layer (HVL). Likewise, the tenth value layer (TVL) specifies the thickness of material required to reduce radiation intensity to 10 % of its initial value (Chikkegowda et al., 2024b), (Reddy et al., 2022). HVL and TVL values were determined using the following equations.

$$HVL = ln(2)/\ \mu \tag{3}$$

$$TVL = ln(10)\ /\ \mu \tag{4}$$

The attenuation of radiation mainly depends on the atomic number and the density of the shielding material. To obtain the density independent attenuation parameter, Beer-Lambert's law can be modified as (Swinehart, 1962),

$$I = I_0\ \ e^{-(\mu/\rho)\rho t} \tag{5}$$

Taking ln on both sides, we get

$$lnI = lnI_0 - (\mu\ /\ \rho)\rho t \tag{6}$$

Thus, the magnitude of the slope of the plot lnI versus ρt directly gives the mass attenuation coefficient μ/ρ (Chikkegowda et al., 2024c), (Reddy et al., 2021). Higher slope indicates a higher value of μ/ρ, indicating a better shielding property.

In a compound or mixture of elements, the average number of atoms interacting with the radiation is indicated by the parameter, effective atomic number (Z_{eff}). Z_{eff} is the ratio of (σ_a) and (σ_{el}) , represented as

$$Z_{eff} = \frac{(\sigma_a)}{(\sigma_{el})} \tag{7}$$

Where σ_a is atomic cross-section and σ_{el} is the electronic cross-section, which represent the probabilities of gamma ray photons interacting with the nucleus and electrons, respectively. It changes according to the gamma ray energy and characterizes multi-element samples in terms of equivalent elements (Sankarshan et al., 2017, 2020; Gowda et al., 2005; Krishnaveni and Gowda, 2005). In terms of mass attenuation coefficient of individual constituent elements of the sample, Z_{eff}, is given by,

$$Z_{eff} = \frac{\Sigma_i n_i A_i (\mu/\rho)_i}{\Sigma_i \frac{n_i A_i}{Z_i} (\mu/\rho)_i} \tag{8}$$

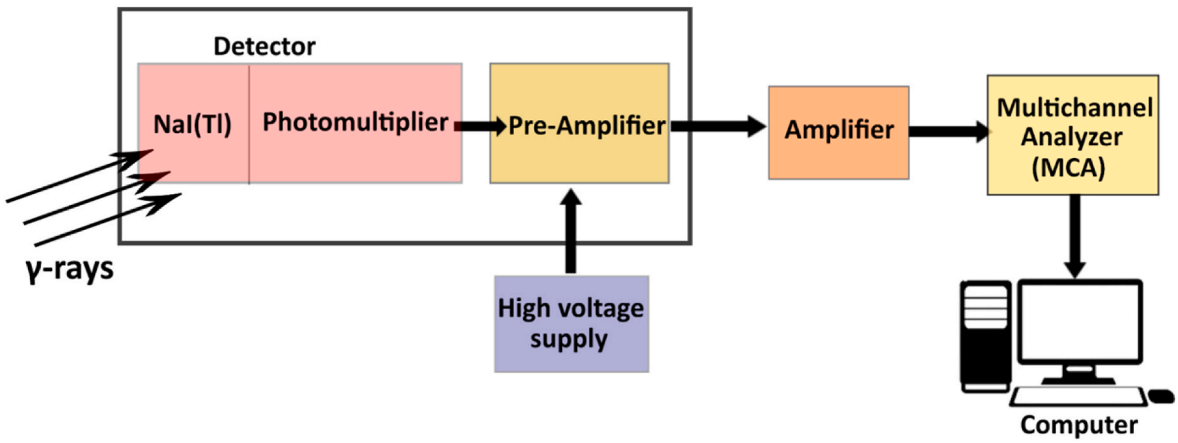

Fig. 3. Schematic representation of gamma ray spectrometer experimental setup.

where the atomic number, number of formula units, atomic weight and mass attenuation coefficient of the i^{th} constituent element are represented as Z_i, n_i, A_i, and $(\mu/\rho)_i$, respectively (Sankarshan and Umesh, 2018).

3. Experimental details

For synthesizing PVA composites, laboratory grade PVA powder (99.99 % pure) was used without any further purification. Glass powder was recovered from broken household glassware. Granite and redmud were obtained from a construction site in Mysore district, Karnataka, India. A PVA solution (6.54 wt%) was prepared using 100 ml distilled water in a beaker and heated at a uniform temperature of 60 °C, stirred continuously using a magnetic stirrer at 400 rpm to obtain a clear solution. Each filler in powder form was added at this stage and with continuous stirring at 60 °C, a homogeneous PVA composite solution was obtained with varying filler concentration of 10, 20, 30, 40 (wt.%). The prepared PVA–Granite, PVA–Glass and PVA–Redmud composite solutions were transferred into separate Petri dishes and kept for drying at room temperature for 2 days. To ensure experimental reliability, three sets of PVA composites (0–40 wt%) were prepared. The films were peeled off after drying and resized in dimensions of 2 x 3 cm^2. The schematic diagram of sample preparation is depicted in Fig. 2. The thickness of each film was measured at multiple points using a screw gauge, where average sample thickness ranged from 0.10 to 0.20 cm.

Synthesized PVA composite films were subjected to gamma ray interaction studies. A calibrated gamma ray spectrometer housing a thallium-activated sodium iodide scintillation detector coupled with multichannel analyzer (MCA)-based computer is used to measure gamma ray intensity, using ^{22}Na (511 keV), ^{137}Cs (661.6 keV) and ^{60}Co (1173 and 1332 keV) gamma sources (Fig. 3). PHAST software from the Bhabha Atomic Research Centre (BARC), Mumbai, India, was utilized to attain gamma ray spectrum. The linearity of the spectrometer was checked initially, and the acquisition time was set to obtain 10^5 to 10^6 counts under the photo peak. Gamma-ray shielding parameters were evaluated using the area under photo peak, obtained with the help of the Gaussian peak fitting routine. The composition of the samples was determined using Energy dispersive spectroscopy (EDS), which is further used in the theoretical calculations of gamma ray attenuation parameters using XCOM and AutoZeff software.

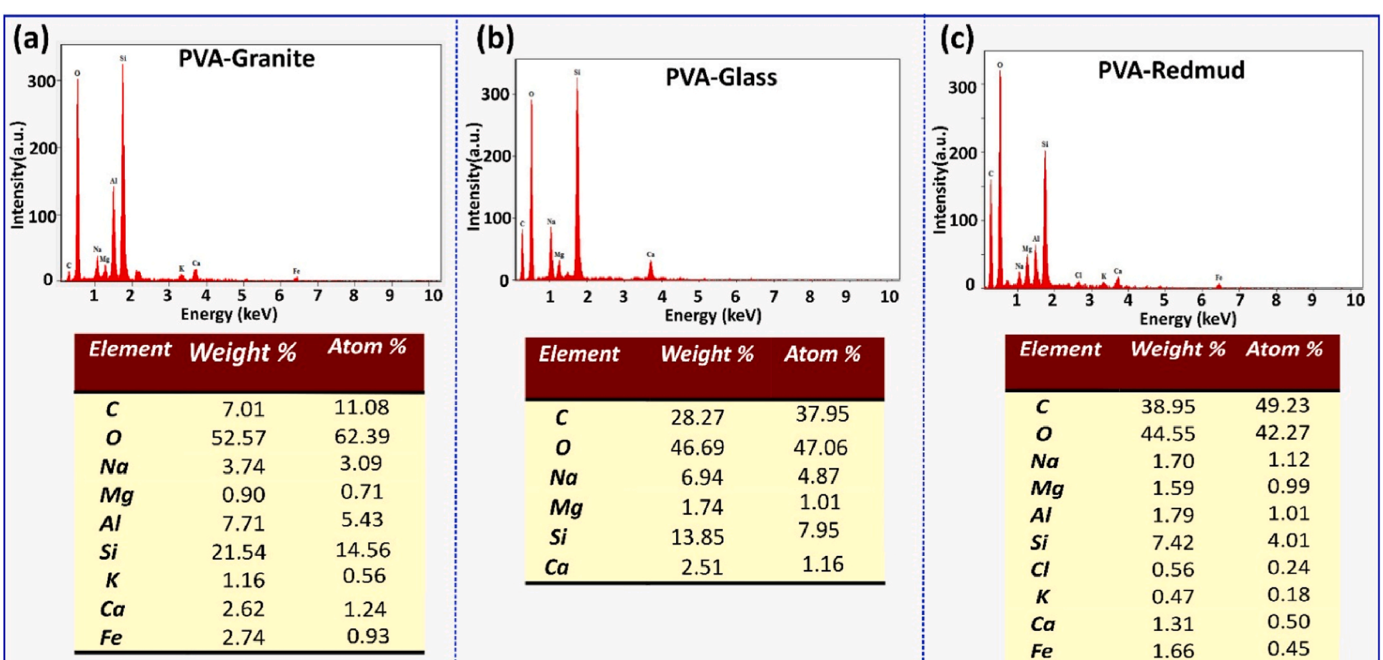

(a) PVA-Granite

Element	Weight %	Atom %
C	7.01	11.08
O	52.57	62.39
Na	3.74	3.09
Mg	0.90	0.71
Al	7.71	5.43
Si	21.54	14.56
K	1.16	0.56
Ca	2.62	1.24
Fe	2.74	0.93

(b) PVA-Glass

Element	Weight %	Atom %
C	28.27	37.95
O	46.69	47.06
Na	6.94	4.87
Mg	1.74	1.01
Si	13.85	7.95
Ca	2.51	1.16

(c) PVA-Redmud

Element	Weight %	Atom %
C	38.95	49.23
O	44.55	42.27
Na	1.70	1.12
Mg	1.59	0.99
Al	1.79	1.01
Si	7.42	4.01
Cl	0.56	0.24
K	0.47	0.18
Ca	1.31	0.50
Fe	1.66	0.45

Fig. 4. EDS and elemental composition of (a) PVA-Granite (b) PVA-Glass, and (c) PVA-Redmud with a filler concentration of 40 wt%.

Table 1
Experimental and theoretical shielding parameters for PVA-Granite composite.

Granite (wt.%)	Energy (keV)	μ/ρ (cm^2/g)		μ (cm^{-1})		HVL (cm)		TVL (cm)		λ (cm)		Z_{eff}	
		Exp.	Th.	Exp.	Th.	Exp.	Th.	Exp.	Th.	Exp.	Th.	Exp.	Th.
0	511	0.085 ± 0.004	0.086	0.183 ± 0.009	0.186	3.78 ± 0.189	3.736	12.56 ± 0.628	12.414	5.454 ± 0.273	5.39	6.559 ± 0.328	6.752
	661.6	0.076 ± 0.004	0.077	0.16 ± 0.008	0.163	4.319 ± 0.216	4.263	14.354 ± 0.718	14.167	6.233 ± 0.312	6.152	6.563 ± 0.328	6.75
	1173	0.058 ± 0.003	0.059	0.122 ± 0.006	0.124	5.697 ± 0.285	5.61	18.933 ± 0.947	18.644	8.221 ± 0.411	8.095	6.588 ± 0.329	6.75
	1332	0.055 ± 0.003	0.055	0.116 ± 0.006	0.116	5.968 ± 0.298	5.968	19.834 ± 0.992	19.834	8.612 ± 0.431	8.612	6.658 ± 0.333	6.75
10	511	0.082 ± 0.004	0.086	0.201 ± 0.01	0.212	3.444 ± 0.172	3.269	11.446 ± 0.572	10.863	4.97 ± 0.249	4.717	7.629 ± 0.381	7.994
	661.6	0.073 ± 0.004	0.077	0.182 ± 0.009	0.192	3.807 ± 0.19	3.609	12.651 ± 0.633	11.995	5.493 ± 0.275	5.208	7.612 ± 0.381	7.998
	1173	0.056 ± 0.003	0.059	0.139 ± 0.007	0.147	4.968 ± 0.248	4.714	16.51 ± 0.826	15.667	7.169 ± 0.358	6.803	7.709 ± 0.385	7.996
	1332	0.052 ± 0.003	0.055	0.13 ± 0.007	0.137	5.329 ± 0.266	5.058	17.711 ± 0.886	16.81	7.69 ± 0.385	7.299	7.608 ± 0.38	7.997
20	511	0.082 ± 0.004	0.086	0.198 ± 0.01	0.208	3.508 ± 0.175	3.332	11.658 ± 0.583	11.072	5.062 ± 0.253	4.808	8.498 ± 0.425	8.912
	661.6	0.073 ± 0.004	0.077	0.179 ± 0.009	0.188	3.877 ± 0.194	3.686	12.885 ± 0.644	12.25	5.595 ± 0.28	5.319	8.482 ± 0.424	8.907
	1173	0.056 ± 0.003	0.059	0.137 ± 0.007	0.144	5.06 ± 0.253	4.812	16.816 ± 0.841	15.993	7.302 ± 0.365	6.944	8.556 ± 0.428	8.902
	1332	0.052 ± 0.003	0.055	0.128 ± 0.006	0.134	5.428 ± 0.271	5.172	18.039 ± 0.902	17.187	7.833 ± 0.392	7.463	8.478 ± 0.424	8.902
30	511	0.09 ± 0.005	0.086	0.209 ± 0.01	0.199	3.316 ± 0.166	3.482	11.02 ± 0.511	11.573	4.785 ± 0.239	5.025	9.383 ± 0.469	8.912
	661.6	0.081 ± 0.004	0.077	0.187 ± 0.009	0.178	3.704 ± 0.185	3.893	12.308 ± 0.615	12.938	5.344 ± 0.267	5.618	9.469 ± 0.473	8.907
	1173	0.062 ± 0.003	0.059	0.143 ± 0.007	0.137	4.834 ± 0.242	5.058	16.063 ± 0.803	16.81	6.975 ± 0.349	7.299	9.53 ± 0.477	8.902
	1332	0.058 ± 0.003	0.055	0.134 ± 0.007	0.127	5.185 ± 0.259	5.457	17.232 ± 0.862	18.134	7.482 ± 0.374	7.874	9.514 ± 0.476	8.902
40	511	0.09 ± 0.005	0.086	0.277 ± 0.014	0.264	2.501 ± 0.125	2.625	8.312 ± 0.416	8.723	3.609 ± 0.18	3.788	9.921 ± 0.496	9.441
	661.6	0.081 ± 0.004	0.077	0.248 ± 0.012	0.236	2.794 ± 0.14	2.936	9.284 ± 0.464	9.758	4.031 ± 0.202	4.237	10.016 ± 0.501	9.436
	1173	0.061 ± 0.003	0.058	0.187 ± 0.009	0.178	3.709 ± 0.185	3.893	12.325 ± 0.616	12.938	5.352 ± 0.268	5.618	9.922 ± 0.496	9.429
	1332	0.058 ± 0.003	0.055	0.177 ± 0.009	0.169	3.911 ± 0.196	4.101	12.998 ± 0.65	13.627	5.644 ± 0.282	5.917	10.068 ± 0.503	9.428

Table 2
Experimental and theoretical shielding parameters for PVA-Glass composite.

Glass (wt.%)	Energy (keV)	μ/ρ (cm^2/g)		μ (cm^{-1})		HVL (cm)		TVL (cm)		λ (cm)		Z_{eff}	
		Exp.	Th.	Exp.	Th.	Exp.	Th.	Exp.	Th.	Exp.	Th.	Exp.	Th.
0	511	0.085 ± 0.004	0.086	0.183 ± 0.009	0.186	3.780 ± 0.189	3.736	12.56 ± 0.628	12.414	5.454 ± 0.273	5.39	6.559 ± 0.328	6.752
	661.6	0.076 ± 0.004	0.077	0.160 ± 0.008	0.163	4.319 ± 0.216	4.263	14.354 ± 0.718	14.167	6.233 ± 0.312	6.152	6.563 ± 0.328	6.75
	1173	0.058 ± 0.003	0.059	0.122 ± 0.006	0.124	5.697 ± 0.285	5.61	18.933 ± 0.947	18.644	8.221 ± 0.411	8.095	6.588 ± 0.329	6.75
	1332	0.055 ± 0.003	0.055	0.116 ± 0.006	0.116	5.968 ± 0.298	5.968	19.834 ± 0.992	19.834	8.612 ± 0.431	8.612	6.658 ± 0.333	6.75
10	511	0.082 ± 0.004	0.086	0.258 ± 0.013	0.271	2.69 ± 0.134	2.555	8.939 ± 0.447	8.493	3.882 ± 0.194	3.688	7.005 ± 0.35	7.34
	661.6	0.073 ± 0.004	0.077	0.230 ± 0.012	0.242	3.011 ± 0.151	2.86	10.006 ± 0.5	9.506	4.345 ± 0.217	4.128	6.984 ± 0.349	7.338
	1173	0.056 ± 0.003	0.059	0.175 ± 0.009	0.184	3.955 ± 0.198	3.757	13.143 ± 0.657	12.486	5.707 ± 0.285	5.421	7.046 ± 0.352	7.336
	1332	0.052 ± 0.003	0.055	0.164 ± 0.008	0.173	4.221 ± 0.211	4.01	14.027 ± 0.701	13.326	6.091 ± 0.305	5.786	6.975 ± 0.349	7.337
20	511	0.082 ± 0.004	0.086	0.252 ± 0.013	0.265	2.755 ± 0.138	2.617	9.155 ± 0.458	8.698	3.975 ± 0.199	3.777	7.058 ± 0.353	7.42
	661.6	0.081 ± 0.004	0.077	0.248 ± 0.012	0.236	2.794 ± 0.14	2.933	9.284 ± 0.464	9.748	4.031 ± 0.202	4.233	7.809 ± 0.39	7.418
	1173	0.062 ± 0.003	0.059	0.189 ± 0.009	0.18	3.665 ± 0.183	3.848	12.178 ± 0.609	12.787	5.288 ± 0.264	5.552	7.861 ± 0.393	7.416
	1332	0.052 ± 0.003	0.055	0.160 ± 0.008	0.169	4.323 ± 0.216	4.107	14.366 ± 0.718	13.647	6.238 ± 0.312	5.926	7.031 ± 0.352	7.416
30	511	0.082 ± 0.004	0.086	0.237 ± 0.012	0.249	2.924 ± 0.146	2.778	9.717 ± 0.486	9.231	4.219 ± 0.211	4.008	7.325 ± 0.366	7.685
	661.6	0.073 ± 0.004	0.077	0.211 ± 0.011	0.223	3.277 ± 0.164	3.113	10.89 ± 0.545	10.346	4.729 ± 0.236	4.492	7.304 ± 0.365	7.682
	1173	0.056 ± 0.003	0.059	0.161 ± 0.008	0.17	4.299 ± 0.215	4.084	14.286 ± 0.714	13.571	6.203 ± 0.31	5.893	7.369 ± 0.368	7.679
	1332	0.058 ± 0.003	0.055	0.167 ± 0.008	0.159	4.151 ± 0.208	4.358	13.795 ± 0.69	14.484	5.99 ± 0.299	6.289	8.136 ± 0.407	7.68
40	511	0.091 ± 0.005	0.086	0.26 ± 0.013	0.248	2.665 ± 0.133	2.799	8.857 ± 0.443	9.3	3.846 ± 0.192	4.038	8.514 ± 0.426	8.04
	661.6	0.073 ± 0.004	0.077	0.21 ± 0.011	0.221	3.298 ± 0.165	3.133	10.959 ± 0.548	10.411	4.759 ± 0.238	4.521	7.653 ± 0.383	8.037
	1173	0.056 ± 0.003	0.059	0.160 ± 0.008	0.168	4.333 ± 0.217	4.117	14.401 ± 0.72	13.68	6.253 ± 0.313	5.94	7.72 ± 0.386	8.033
	1332	0.058 ± 0.003	0.055	0.166 ± 0.008	0.158	4.185 ± 0.209	4.394	13.907 ± 0.695	14.602	6.039 ± 0.302	6.341	8.527 ± 0.426	8.343

Table 3
Experimental and theoretical shielding parameters for PVA-redmud composite.

Redmud (wt.%)	Energy (keV)	μ/ρ (cm^2/g)		μ (cm^{-1})		HVL (cm)		TVL (cm)		λ (cm)		Z_{eff}	
		Exp.	Th.	Exp.	Th.	Exp.	Th.	Exp.	Th.	Exp.	Th.	Exp.	Th.
0	511	0.085 ± 0.004	0.086	0.183 ± 0.009	0.186	3.78 ± 0.189	3.736	12.56 ± 0.628	12.414	5.454 ± 0.273	5.39	6.559 ± 0.328	6.752
	661.6	0.076 ± 0.004	0.077	0.16 ± 0.008	0.163	4.319 ± 0.216	4.263	14.354 ± 0.718	14.167	6.233 ± 0.312	6.152	6.563± 0.328	6.75
	1173	0.058 ± 0.003	0.059	0.122 ± 0.006	0.124	5.697 ± 0.285	5.61	18.933 ± 0.947	18.644	8.221 ± 0.411	8.095	6.588 ± 0.329	6.75
	1332	0.055 ± 0.003	0.055	0.116 ± 0.006	0.116	5.968 ± 0.298	5.968	19.834 ± 0.992	19.834	8.612 ± 0.431	8.612	6.658 ± 0.333	6.75
10	511	0.082 ± 0.004	0.086	0.265 ± 0.013	0.278	2.615 ± 0.131	2.493	8.689 ± 0.434	8.285	3.773 ± 0.189	3.597	6.715 ± 0.336	7.052
	661.6	0.073 ± 0.004	0.077	0.236 ± 0.012	0.249	2.937 ± 0.147	2.784	9.76 ± 0.488	9.253	4.238 ± 0.212	4.018	6.694 ± 0.335	7.051
	1173	0.055 ± 0.003	0.059	0.178 ± 0.009	0.191	3.898 ± 0.195	3.634	12.954 ± 0.648	12.076	5.625 ± 0.281	5.244	6.633 ± 0.332	7.05
	1332	0.052 ± 0.003	0.055	0.169 ± 0.008	0.178	4.096 ± 0.205	3.898	13.611 ± 0.681	12.954	5.91 ± 0.296	5.625	6.731 ± 0.337	7.05
20	511	0.082 ± 0.004	0.086	0.256 ± 0.013	0.269	2.707 ± 0.135	2.581	8.994 ± 0.45	8.576	3.906 ± 0.195	3.724	6.718 ± 0.336	7.067
	661.6	0.073 ± 0.004	0.077	0.229 ± 0.011	0.24	3.03 ± 0.152	2.882	10.07 ± 0.503	9.578	4.372 ± 0.219	4.159	6.719 ± 0.336	7.065
	1173	0.061 ± 0.003	0.059	0.19 ± 0.01	0.184	3.638 ± 0.182	3.762	12.091 ± 0.605	12.501	5.25 ± 0.263	5.428	7.359 ± 0.368	7.065
	1332	0.058 ± 0.003	0.055	0.181 ± 0.009	0.172	3.836 ± 0.192	4.035	12.748 ± 0.637	13.41	5.535 ± 0.277	5.823	7.442 ± 0.372	7.066
30	511	0.091 ± 0.005	0.086	0.287 ± 0.014	0.273	2.411 ± 0.121	2.541	8.013 ± 0.401	8.443	3.479 ± 0.174	3.666	7.598 ± 0.38	7.224
	661.6	0.073 ± 0.004	0.077	0.232 ± 0.012	0.244	2.983 ± 0.149	2.838	9.913 ± 0.496	9.43	4.305 ± 0.215	4.095	6.878 ± 0.344	7.222
	1173	0.055 ± 0.003	0.059	0.174 ± 0.009	0.187	3.973 ± 0.199	3.703	13.202 ± 0.66	12.307	5.732 ± 0.287	5.344	6.792 ± 0.34	7.222
	1332	0.052 ± 0.003	0.055	0.166 ± 0.008	0.174	4.182 ± 0.209	3.973	13.897 ± 0.695	13.202	6.034 ± 0.302	5.732	6.882 ± 0.344	7.222
40	511	0.082 ± 0.004	0.086	0.252 ± 0.013	0.264	2.755 ± 0.138	2.626	9.155 ± 0.458	8.728	3.975 ± 0.199	3.79	7.218 ± 0.361	7.572
	661.6	0.073 ± 0.004	0.077	0.224 ± 0.011	0.236	3.09 ± 0.154	2.933	10.268 ± 0.513	9.748	4.459 ± 0.223	4.233	7.209 ± 0.36	7.569
	1173	0.0620 ± 0.003	0.059	0.189 ± 0.009	0.181	3.673 ± 0.184	3.828	12.205 ± 0.61	12.722	5.3 ± 0.265	5.524	7.979 ± 0.399	7.565
	1332	0.058 ± 0.003	0.055	0.177 ± 0.009	0.169	3.911 ± 0.196	4.107	12.998 ± 0.65	13.647	5.644 ± 0.282	5.926	7.988 ± 0.399	7.566

4. Results and discussion

In this study, PVA composite samples such as PVA-Granite, PVA-Glass and PVA-Redmud with different filler concentrations have been synthesized by the solution casting method. To know the elemental composition, the synthesized films were characterized by Energy dispersive spectroscopy. Fig. 4(a–c) show the EDS and the corresponding atomic % and weight % of elements present in PVA-Granite, PVA-Glass and PVA-Redmud composites for 40 wt% filler concentration, respectively.

In the present work we have examined the radiation shielding properties of PVA-Granite, PVA-Glass and PVA-Redmud composites by evaluating several key shielding parameters such as linear attenuation coefficient (μ), mass attenuation coefficient (μ/ρ), half value layer (HVL), tenth value layer (TVL), mean free path (λ), and effective atomic number (Z_{eff}), using both experimental and theoretical methods.

From the experiment, gamma ray spectra for samples of different compositions of fillers for different thicknesses were obtained. The transmitted intensity (I) recorded using a PC-based MCA was obtained using PHAST software. The mass and dimensions of each of these samples were used to calculate mass thickness (ρt). The logarithm of intensity, $ln\ (I)$ is plotted against ρt and the slope of the resulting line is used to determine the μ/ρ. Theoretically, μ/ρ values were computed using XCOM (version 3.1) software developed by NIST (National Institute of Standards and Technology) (MJ, 1998). The software utilizes a detailed database of atomic cross sections that explain how radiation interacts with various substances. Both theoretical and experimental values obtained for PVA-Granite, PVA-Glass and PVA-Redmud samples of different percentage compositions at energies 511, 661.6, 1173, and 1332 keV are reported in Tables 1–3. These theoretical data were found to agree well with experimental values within experimental errors. μ is obtained by multiplying μ/ρ with the sample density. With the help of these μ values, λ, HVL, and TVL values are determined using equations (2)–(4), respectively.

The experimentally obtained μ/ρ is used to obtain the atomic/molecular interaction cross section of the particular material. The electronic cross section is calculated from the theoretical values of μ/ρ and the elemental composition of the material obtained by EDS data. This information is then used to determine the Z_{eff} of the samples using equation (7) to assess the sample effectiveness in shielding against gamma radiation. Theoretical calculations of Z_{eff} were carried out using AutoZeff software (version 1.7) (Taylor et al., 2012), which considers the atomic composition and weight percentages of elements in a sample. It calculates Z_{eff} as a weighted average based on the interaction probabilities of different elements. The software also incorporates the energy of the incident radiation, which is essential for accurate results. The experimental errors in determining the gamma ray interaction parameters mainly arise from sample geometry and gamma ray intensity measurements. The overall experimental uncertainty in the measured shielding parameters was estimated to be approximately ∼5 %, calculated using the root-sum-square method. The primary sources of uncertainty included counting statistics (0.6 %), which arise from the $\sqrt{N}$ dependence of photon counting; sample thickness variation (1.0 %), determined from multiple measurements across each film; and density determination (1.5 %), due to slight errors in mass and volume measurements. Additional uncertainties were contributed by detector calibration and efficiency (2.0 %), reflecting instrumental and energy-dependent variations; sample inhomogeneity (3.0 %), caused by non-uniform filler dispersion and surface irregularities; geometry and alignment (0.5 %), from minor deviations in source-to-detector positioning; and electronic or systematic factors (2.0 %), associated with background subtraction, dead time, and energy resolution. Combining these factors yields a total experimental uncertainty of about 5 %, which is within acceptable limits for gamma-ray attenuation measurements. The experimental gamma ray attenuation parameters along with the experimental errors and the theoretical values for these parameters for

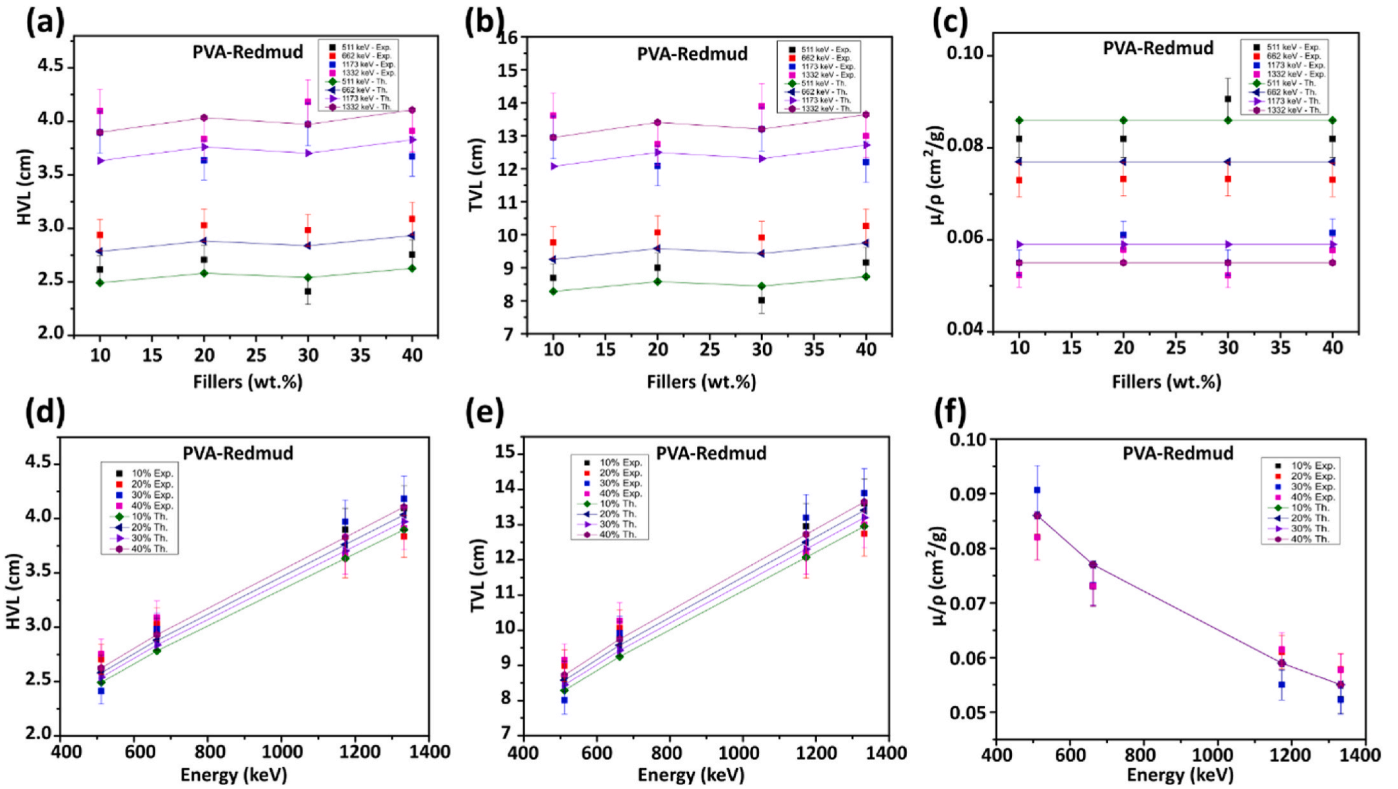

Fig. 5. (a) HVL, (b) TVL and (c) μ/ρ versus filler concentration, (d) HVL, (e) TVL and (f) μ/ρ versus energy of the gamma source, respectively, for PVA-Redmud composite.

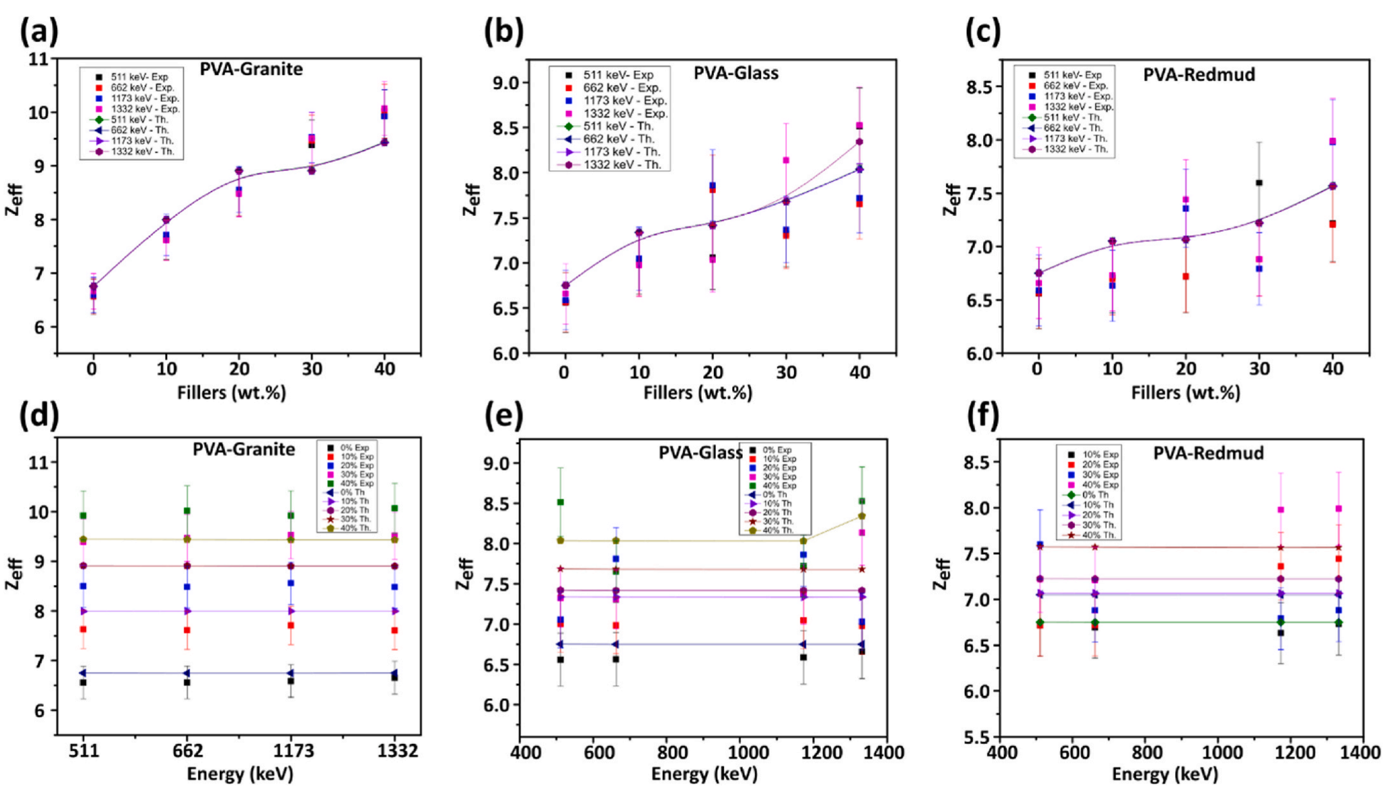

Fig. 6. Z_{eff} plotted against, filler concentration for (a) PVA-Granite, (b) PVA- Glass, and (c) PVA-Redmud composites and Z_{eff} plotted against energy of the photons for (d) PVA-Granite, (e) PVA- Glass, and (f) PVA-Redmud composites, respectively.

three sets of samples are calculated and the best data among them are provided in Tables 1–3, for PVA-Granite, PVA-Glass and PVA-Redmud for different compositions at gamma ray energies, 511, 661.6, 1173, and 1332 keV, respectively.

From the data, it is observed that experimental values of shielding parameters for PVA-Granite, PVA-Glass, and PVA-Redmud, agree well with theoretical values within the limit of experimental errors. It is worth noting that, μ, μ/ρ and Z_{eff} increased significantly, whereas λ, HVL and TVL decreased with increase in filler concentration from 0 to 40 wt % of fillers in composites for the energies of present interest. A typical representation of the plot of HVL, TVL and μ/ρ, versus percentage fillers and gamma energies of present interest, for PVA-Redmud composite is as shown in Fig. 5(a–f), respectively. The experimental and theoretical values in the plots are denoted by dots and lines, respectively, with experimental errors as error bars. Fig. 6(a–f), depicts the plot of Z_{eff} versus percentage of fillers and energy for PVA-Granite, PVA-Glass and PVA-Redmud, respectively.

At 40 wt%, the increased content of the filler leads to greater photon attenuation, resulting in reduced penetration depth. For example, in the case of gamma ray energy at 511 keV, HVL decrease to 2.501, 2.665, and 2.755 cm for PVA-Granite, PVA-glass, and PVA-Redmud compared to 3.78 cm at 0 wt%, showing a substantial improvement. Similarly, the TVL also reduce to 8.312, 8.857 and 9.155 cm for PVA-Granite, PVA-glass, and PVA-Redmud, respectively. This confirms that increasing the weight percentage of the fillers significantly improves the shielding capacity by requiring less material to achieve the same attenuation. Lower values of the HVL and TVL at 40 wt% for all composites, PVA-Granite, PVA-Glass, and PVA-Redmud, indicate enhanced radiation shielding effectiveness at higher filler concentrations. Among 40 wt % of PVA-composites, PVA-Granite composite exhibited the highest μ/ρ and Z_{eff} across all energies compared to PVA-Glass and PVA-Redmud. From the experimentally obtained values provided in Tables 1–3, it is observed that, the highest change in the parameters with respect to pristine PVA (0 wt%) varies in the following manner. μ/ρ, μ, HVL, TVL, and λ, varied from 0.085 to 0.090 cm^2/g, 0.183 to 0.277 cm^{-1}, 3.780 to 2.501 cm, 12.560 to 8.312 cm, and 5.454 to 3.309 cm, respectively, at 511 keV, whereas, Z_{eff} varied from 6.559 to 10.068 at 1332 keV, for PVA-Granite 40 wt% with an estimated experimental error of 5 %. Hence, PVA-Granite exhibited a highest shielding performance compared to PVA-Glass, and PVA-Redmud. Further, with increase in energy, μ/ρ and μ decreases, HVL, TVL, and λ increases, whereas Z_{eff} remains almost constant. The constant Z_{eff} values with increasing energy in the range of 0.1–1 MeV is attributed to the dominance of Compton scattering, which is linearly dependent on the atomic number (Z) of the elements in the material.

5. Conclusion

In the present study PVA-based composites reinforced with granite, glass, and redmud fillers have been successfully fabricated and characterized to evaluate their gamma radiation shielding properties. The incorporation of fillers significantly enhanced the shielding performance, particularly at higher filler concentrations. The essential parameters like μ, μ/ρ, λ, HVL, TVL and Z_{eff} were determined. The experimentally determined parameters were compared with theoretical values obtained using EDS data and found to agree with theoretical values within an experimental error of ~5 %. Therefore, the attenuation studies demonstrated that μ, μ/ρ and Z_{eff} increased, whereas λ, HVL and TVL decreased with an increasing amount of fillers (0–40 wt%) for all energies of present interest. On the other hand, as the energy of the source increased, μ, μ/ρ and Z_{eff} decreased, whereas λ, HVL and TVL increased. The maximum values of μ/ρ i.e., 0.090, 0.089, and 0.082 cm^2/g were observed at 511 keV for PVA–Granite, PVA–Glass, and PVA–Redmud composites, respectively, at a 40 wt% filler concentration. Correspondingly, Z_{eff} values at 1332 keV were found to be 10.068, 8.527, and 7.988 for the same composites. The maximum percentage deviation is observed in PVA–Granite, i.e., increasing the filler content from 0 to 40 wt%, reduced the HVL by 33.8 %, TVL by 33.8 %, and λ by 33.8 %, while μ increased by 51.9 % and Z_{eff} by 51.2 %. Hence, among the composites studied, PVA- Granite exhibited superior gamma attenuation properties, followed by PVA-Glass and PVA-Redmud. These findings reveal that PVA composites reinforced with waste materials such as granite, glass, and red mud as fillers with PVA can serve as lightweight, flexible, and eco-friendly sustainable alternative materials to conventional lead-based shielding materials, and have potential applications in medical imaging facilities, nuclear power plants and other radiation prone industrial environments. Future studies could be focused on optimizing the filler composition to further enhance shielding performance, along with comprehensive evaluation of mechanical properties to ensure structural integrity under practical conditions. In addition, long-term durability assessments, including the effects of environmental exposure and radiation aging, could be conducted to validate real-world stability.

CRediT authorship contribution statement

Ashwitha Chikkegowda: Writing – original draft, Methodology, Investigation, Formal analysis, Data curation. **Adarsh Raj Lingaraj:** Writing – original draft, Visualization, Methodology, Investigation, Formal analysis, Conceptualization. **Vaishnavi Narayan:** Writing – original draft, Visualization, Methodology, Investigation, Formal analysis, Conceptualization. **Sankarshan Belur Mohan:** Writing – review & editing, Visualization, Validation, Supervision, Software, Resources, Project administration. **Sannathammegowda Krishnaveni:** Writing – review & editing, Validation, Supervision, Software, Resources, Project administration, Methodology, Conceptualization.

Declaration of AI-assisted technologies in the writing process

During the preparation of this work, the authors used ChatGPT to improve language and readability. After using this tool, the authors reviewed and edited the content as needed and take full responsibility for the content of the publication.

Declaration of competing interest

The authors declare that they have no known competing financial interests or personal relationships that could have appeared to influence the work reported in this paper.

Acknowledgments

This paper is based on the authors' research work carried out at Department of Studies in Physics, Manasagangotri, University of Mysore and is gratefully acknowledged. L Adarsh Raj acknowledges the Karnataka Science and Technology Promotion Society (KSTePS), for providing financial support under DST-Ph.D. fellowship (Award letter No. DST/KSTePS/Ph.D. Fellowship/MP -05:2023–24/433). Vaishnavi N. acknowledges OBC-Cell, University of Mysore, for providing financial assistance under UoM-OBC Fellowship (Award letter No. Order No. OBC CELL-01/08/2020-21/120: Dated: March 15, 2025).

Data availability

Data will be made available on request.

References

Abdalla, A.M., Al-Naggar, T.I., Bashiri, A.M., Alsareii, S.A., 2022. Radiation shielding performance for local granites. Prog. Nucl. Energy 150, 104294.
Agool, I.R., Kadhim, K.J., Hashim, A., 2017. Synthesis of (PVA–PEG–PVP–ZrO 2) nanocomposites for energy release and gamma shielding applications. Int. J. Plast. Technol. 21, 444–453.

Ahmad, M.I., Rahim, M. H. Ab, Nordin, R., Mohamed, F., Abu-Samah, A., Abdullah, N.F., 2021. Ionizing radiation monitoring technology at the verge of internet of things. Sensors 21 (22), 7629.
Aita, R.S., Ghany, H.A.A., Ibrahim, E.M., El-Feky, M.G., El Aassy, I.E., Mahmoud, K.A., 2022. Gamma-rays attenuation by mineralized siltstone and dolostone rocks: Monte Carlo simulation, theoretical and experimental evaluations. Radiat. Phys. Chem. 198, 110281.
Al-Buriahi, M.S., Alsaiari, N.S., Baskin, M.U., Olarinoye, I.O., 2025. Recent progress in the radiation shielding performance of common glass systems: the roles of different class of modifiers. J. Radiat. Res. Appl. Sci. 18 (1), 101264.
Alabsy, M.T., Gouda, M.M., Abbas, M.I., Al-Balawi, S.M., El-Khatib, A.M., 2023. Enhancing the gamma-radiation-shielding properties of gypsum–lime–waste marble mortars by incorporating micro-and nano-PbO particles. Materials 16 (4), 1577.
Alomayrah, N., Al-Buriahi, M.S., 2024. Optical properties, gamma attenuation and fast neutrons moderating performance of V2O5–Bi2O3–B2O3–PbO glasses. J. Australas. Ceram. Soc. 1–11.
Alrowaili, Z.A., Alsaiari, N.S., İbrahimoğlu, E., Çalışkan, F., Olarinoye, I.O., Al-Buriahi, M.S., 2024. Physical, chemical and radiation shielding properties of metakaolin-based geopolymers containing borosilicate waste glass. Radiat. Phys. Chem. 224, 112075.
Alrowaili, Z.A., et al., 2025. Gamma attenuation, buildup factors, and radiation shielding performance of CaO-borosilicate glasses. J. Radiat. Res. Appl. Sci. 18 (1), 101221.
Alsaiari, N.S., Alsufyani, S.J., Alrowaili, Z.A., Eke, C., Sriwunkum, C., Al-Buriahi, M.S., 2025a. Radiation attenuation, dose rate and buildup factors of gallium silicate glass system for nuclear shielding applications. Radiat. Phys. Chem. 229, 112500.
Alsaiari, N.S., Iliyasu, U., Ibrahimoglu, E., Al-Buriahi, M.S., 2025b. Influence of Bi2O3 and Y2O3 co-doping on the structural and nuclear shielding properties of multi-elemental based glass-ceramics. Ceram. Int.
Alzahrani, F.M.A., Albarkaty, K.S., Çalişkan, F., Olarinoye, I.O., Al-Buriahi, M.S., 2023. Physical, microstructural, and radiation energy absorption properties of recycled CRT-screen glass doped with Bi2O3. J. Radiat. Res. Appl. Sci. 16 (4), 100727.
Alzahrani, F.M.A., Elqahtani, Z.M., Alzahrani, J.S., Eke, C., Alrowaili, Z.A., Al-Buriahi, M.S., 2024. Gamma attenuation characteristics of silicon-rich glasses in Na2O–SiO2–Al2O3–CaO–ZnO system for radiation applications. J. Radiat. Res. Appl. Sci. 17 (1), 100760.
Ashori, A., Sheshmani, S., 2010. Hybrid composites made from recycled materials: moisture absorption and thickness swelling behavior. Bioresour. Technol. 101 (12), 4717–4720.
Baraker, B.M., Lobo, B., 2018. Microstructure of cadmium chloride doped PVA/PVP blend films. Mater. Today Proc. 5 (1), 3036–3043.
Barman, R., Hossain, M.S., Das, A., Rabby, M.K.A., 2022. Investigation of radiation shielding characteristic features of different wood species. Radiat. Phys. Chem. 192, 109927.
Basu, P., Sarangapani, R., Venkatraman, B., 2019. Gamma ray buildup factors for conventional shielding materials and buildup factors computed for tungsten with a thickness beyond 40 mean free paths. Appl. Radiat. Isot. 154, 108864.
Bel, T., Arslan, C., Baydogan, N., 2019. Radiation shielding properties of poly (methyl methacrylate)/colemanite composite for the use in mixed irradiation fields of neutrons and gamma rays. Mater. Chem. Phys. 221, 58–67.
Bhosale, R.R., More, C.V., Gaikwad, D.K., Pawar, P.P., Rode, M.N., 2017. Radiation shielding and gamma ray attenuation properties of some polymers. Nucl. Technol. Radiat. Protect. 32 (3), 288–293.
Bonifazi, G., Chiara, G., Roberta, P., Silvia, S., 2025. Current trends and challenges in construction and demolition waste recycling. Curr. Opin. Green Sustainable Chem., 101032
Chiang, P.F., et al., 2024. Impacts of polyvinyl alcohol and chitosan-modified biochar on the anaerobic digestion of sewage sludge and valuable resource recovery. Processes 12 (9), 1987.
Chikkegowda, A., Adarsh Raj, L., Belur Mohan, S., Sannathammegowda, K., 2024a. Gamma-ray shielding characteristics of concrete containing different percentage of ceramics for different energies. Radiat. Protect. Dosim. 200 (11–12), 1153–1157.
Chikkegowda, A., Adarsh Raj, L., Belur Mohan, S., Krishnaveni, S., 2024b. Study on polymer composites with glass for gamma ray shielding. Radiat. Protect. Dosim. 200 (11–12), 1233–1236.
Chikkegowda, A., Adarsh Raj, L., Belur Mohan, S., Krishnaveni, S., 2024c. Gamma-ray interaction studies of concrete with waste glass fillers. Radiat. Protect. Dosim. 200 (11–12), 1224–1227.
Chmielewski, A.G., 2010. Chitosan and radiation chemistry. Radiat. Phys. Chem. 79 (3), 272–275.
Daw, S., Basu, R.K., Das, S.K., 2019. Red mud reinforced polyvinyl alcohol composite films: synthesis, chemical, mechanical and thermal properties. SN Appl. Sci. 1 (6), 625.
Echeweozo, E.O., Alomairy, S., Alsaiari, N.S., Al-Buriahi, M.S., 2024. Effect of lead oxide addition on gamma radiation shielding properties of newly developed geopolymers: theoretical and simulation studies. Sci. Rep. 14 (1), 29968.
El-Khayatt, A.M., Saudi, H.A., 2024. Green approach for conversion of hazardous red mud into an efficient transparent neutron and gamma-ray shield. Radiat. Phys. Chem. 215, 111339.
Elgazzar, A.H., Kazem, N., 2014. Biological effects of ionizing radiation. In: The Pathophysiologic Basis of Nuclear Medicine. Springer, pp. 715–726.
Elqahtani, Z.M., Alrowaili, Z.A., Alsaiari, N.S., Alnairi, M.M., Olarinoye, I.O., Al-Buriahi, M.S., 2025. Gamma absorption and radiation shielding properties of apatite-wollastonite containing SiO2, Fe2O3, and TiO2. Radiat. Phys. Chem. 226, 112282.
Elsafi, M., Koraim, Y., Almurayshid, M., Almasoud, F.I., Sayyed, M.I., Saleh, I.H., 2021. Investigation of photon radiation attenuation capability of different clay materials. Materials 14 (21), 6702.
Gowda, S., Krishnaveni, S., Gowda, R., 2005. Studies on effective atomic numbers and electron densities in amino acids and sugars in the energy range 30–1333 keV. Nucl. Instrum. Methods Phys. Res. Sect. B Beam Interact. Mater. Atoms 239 (4), 361–369.
Gual, M.R., Mesquita, A.Z., Pereira, C., 2018. Evaluation of an alternative shielding materials for F-127 transport package. Radiat. Phys. Chem. 144, 29–33.
Henaish, A.M.A., et al., 2020. Spectral, electrical, magnetic and radiation shielding studies of Mg-doped Ni–Cu–Zn nanoferrites. J. Mater. Sci. Mater. Electron. 31, 20210–20222.
Hussain, S., et al., 2022. Modern diagnostic imaging technique applications and risk factors in the medical field: a review. BioMed Res. Int. 2022 (1), 5164970.
Issa, S.A.M., Rashad, M., Hanafy, T.A., Saddeek, Y.B., 2020. Experimental investigations on elastic and radiation shielding parameters of WO3-B2O3-TeO2 glasses. J. Non-Cryst. Solids 544, 120207.
Issa, S.A.M., Zakaly, H.M.H., Pyshkina, M., Mostafa, M.Y.A., Rashad, M., Soliman, T.S., 2021. Structure, optical, and radiation shielding properties of PVA–BaTiO3 nanocomposite films: an experimental investigation. Radiat. Phys. Chem. 180, 109281.
Jia, Z., et al., 1999. Study on poly (methyl methacrylate)/carbon nanotube composites. Mater. Sci. Eng., A 271 (1–2), 395–400.
Junior, T.A.A., Nogueira, M.S., Vivolo, V., Potiens, M.P.A., Campos, L.L., 2017. Mass attenuation coefficients of X-rays in different barite concrete used in radiation protection as shielding against ionizing radiation. Radiat. Phys. Chem. 140, 349–354.
Kaçal, M.R., Akman, F., Sayyed, M.I., 2019. Evaluation of gamma-ray and neutron attenuation properties of some polymers. Nucl. Eng. Technol. 51 (3), 818–824.
Katubi, K.M., et al., 2023. Radiation attenuation and optical properties of P2O5-based glass system. J. Radiat. Res. Appl. Sci. 16 (4), 100688.
Katubi, K.M., et al., 2024. Radiation shielding efficiency of lead-tungsten-boron glasses with Sb, Al, and Bi against gamma, neutron and charge particles. Appl. Radiat. Isot. 204, 111139.
Krishnappa, K., Mohan, S.B., Ankanathappa, S.M., Sannathammegowda, K., 2023. Fabrication of cadmium chloride PVA polymer composite for γ-ray shielding. Radiat. Protect. Dosim. 199 (20), 2487–2490.
Krishnaveni, S., Gowda, R., 2005. Incoherent scattering functions of iron, copper, zirconium, tin, tantalum, tungsten, gold and lead, in the momentum range 2 Å− 1⩽ q⩽ 46 Å− 1 at 661.6 keV photon energy. Nucl. Instrum. Methods Phys. Res. Sect. B Beam Interact. Mater. Atoms 229 (3–4), 333–338.
Madbouly, A.M., et al., 2022. Experimental and FLUKA evaluation on structure and optical properties and γ-radiation shielding capacity of bismuth borophosphate glasses. Prog. Nucl. Energy 148, 104219.
Mahmoud, K.A., Tashlykov, O.L., Mhareb, M.H.A., Almuqrin, A.H., Alajerami, Y.S.M., Sayyed, M.I., 2021. A new heavy-mineral doped clay brick for gamma-ray protection purposes. Appl. Radiat. Isot. 173, 109720.
MJ, B., 1998. Photon cross sections database. NIST Standard Reference Database 8 (XGAM).
Mostafa, M.Y.A., Zakaly, H.M.H., Issa, S.A.M., Saudi, H.A., Henaish, A.M.A., 2022. Tailoring variations in the linear optical and radiation shielding parameters of PVA polymeric composite films doped with rare-earth elements. Appl. Phys. A 128 (3), 199.
Pavlidou, S., Koroneos, A., Papastefanou, C., Christofides, G., Stoulos, S., Vavelides, M., 2006. Natural radioactivity of granites used as building materials. J. Environ. Radioact. 89 (1), 48–60.
Reddy, B.C., et al., 2021. Synthesis and characterization of multi functional nickel ferrite nano-particles for X-ray/gamma radiation shielding, display and antimicrobial applications. J. Phys. Chem. Solid. 159, 110260.
Reddy, B.C., et al., 2022. Synthesis and characterization of Barium ferrite nano-particles for X-ray/gamma radiation shielding and display applications. Prog. Nucl. Energy 147, 104187.
Sakthibala, R.K., Vasanthi, P., Hariharasudhan, C., Partheeban, P., 2025. A Critical Review on Recycling and Reuse of Construction and Demolition Waste Materials. Clean. Waste Syst., 100375
Salati, A., Isfahani, H.S., Rowshanzamir, M.A., Azhari, A., 2022. Effect of red mud additive on the performance of clay barriers for radioactive waste disposals: an experimental study. Arabian J. Geosci. 15 (17), 1467.
Sankarshan, B.M., Umesh, T.K., 2018. Determination of the effective atomic number: a theoretical justification. Europhys. Lett. 123 (2), 27001.
Sankarshan, B.M., Athrey, C.D., Umesh, T.K., 2017. Determination of the effective atomic number of thick samples of unknown composition using scattering studies. Eur. Phys. J. Plus 132 (6), 271.
Sankarshan, B.M., Athrey, C.D., Umesh, T.K., 2020. Effective atomic number for Compton scattering: a benchmark tool to characterize materials. Eur. Phys. J. Plus 135 (4), 344.
Sayyed, M.I., Almurayshid, M., Almasoud, F.I., Alyahyawi, A.R., Yasmin, S., Elsafi, M., 2022a. Developed a new radiation shielding absorber composed of waste marble, polyester, PbCO3, and CdO to reduce waste marble considering environmental safety. Materials 15 (23), 8371.
Sayyed, M.I., Almousa, N., Elsafi, M., 2022b. Green conversion of the hazardous cathode ray tube and red mud into radiation shielding concrete. Materials 15 (15), 5316.
Şengül, A., Akkurt, İ., Gunoglu, K., Akgüngör, K., Ermis, R.B., 2023. Experimental evaluation of gamma-rays shielding properties of ceramic materials used in dentistry. Radiat. Phys. Chem. 204, 110701.
Shwita, F., El-Faramawy, N., Ramadan, W., Ramadan, M., 2021. Investigation of the mechanical properties, morphology and the attenuation behavior of gamma rays for OPC pastes mingled with two different glass wastes. Constr. Build. Mater. 313, 125475.

Singh, P., Kumar, R., 2019. Radiation physics and chemistry of polymeric materials. Radiat. Eff. Polym. Mater. 35–68.
Singh, A.K., Singh, R.K., Sharma, B., Tyagi, A.K., 2017. Characterization and biocompatibility studies of lead free X-ray shielding polymer composite for healthcare application. Radiat. Phys. Chem. 138, 9–15.
Swinehart, D.F., 1962. The beer-lambert law. J. Chem. Educ. 39 (7), 333.
Taylor, M.L., Smith, R.L., Dossing, F., Franich, R.D., 2012. Robust calculation of effective atomic numbers: the Auto-Zeff software. Med. Phys. 39 (4), 1769–1778.
Thangprasert, A., Tansakul, C., Thuaksubun, N., Meesane, J., 2019. Mimicked hybrid hydrogel based on gelatin/PVA for tissue engineering in subchondral bone interface for osteoarthritis surgery. Mater. Des. 183, 108113.
Wang, W., Zheng, B., Deng, Z., Feng, Z., Fu, L., 2013. Kinetics and equilibriums for adsorption of poly (vinyl alcohol) from aqueous solution onto natural bentonite. Chem. Eng. J. 214, 343–354.
Watanabe, Y., 1999. Derivation of linear attenuation coefficients from CT numbers for low-energy photons. Phys. Med. Biol. 44 (9), 2201.
Yang, B., Yang, Y., Huo, Z., Yu, Y., 2023. Advances in research on aging properties of polyvinyl chloride and polyvinylidene fluoride membranes. Constr. Build. Mater. 367, 130292.
Yu, H., et al., 2007. Preparation and luminescent properties of europium-doped yttria fibers by electrospinning. J. Lumin. 124 (1), 39–44.